Alloying Au with Pd suppresses H_2 evolution and promotes selective CO_2 electroreduction to CO at low overpotentials

Supporting Information

Marco Valenti*[1], Nitin P. Prasad[1], Recep Kas[1], Divya Bohra[1], Ming Ma[1], Vignesh Balasubramanian[1], Liangyong Chu[1], Sixto Gimenez [2], Juan Bisquert [2], Bernard Dam[1] & Wilson A. Smith*[1]

[1]Materials for Energy Conversion and Storage (MECS), Department of Chemical Engineering, Faculty of Applied Sciences, Delft University of Technology, Delft 2628-BL, The Netherlands

[2]Photovoltaic and Optoelectronics Devices Group, Departament de Fisica, Universitat Jaume I Av Sos Baynat s/n, 12071, Castello, Spain.

SI-1. Surface Roughness

The surface roughness of the Au-Pd thin films deposited on quartz substrates were characterized by atomic force microscopy (AFM). The images are shown in Figure 1S. The average roughness and the RMS are tabulated in Table 1S.

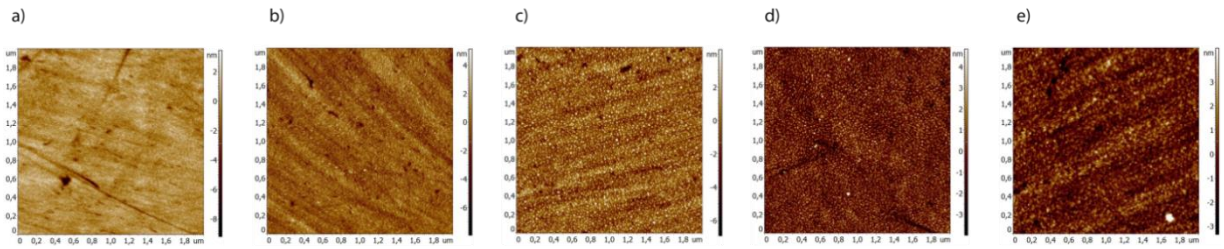

Figure 1S. AFM images for Pd-Au thin film alloys of composition (a) Pd (b) $Au_{25}Pd_{75}$ (c) $Au_{50}Pd_{50}$ (d) $Au_{75}Pd_{25}$ (e) Au

Composition	RMS roughness (nm)	Average roughness (nm)
Au	1.127	0.872
$Au_{75}Pd_{25}$	1.362	1.060
$Au_{50}Pd_{50}$	1.443	1.105
$Au_{25}Pd_{75}$	1.486	1.157
Pd	0.878	0.656

Table 1S. Average roughness and RMS roughness of the surface as calculated using the atomic force microscopy (AFM)

SI-2. Valence band spectra from XPS before and after etching

The valence band spectra of all the electrodes were taken before and after 29 cycles of etching using an ion beam of 500 eV with the Ta_2O_5 estimated sputter rate of 0.02 nm/s. Each etch cycle lasted for 1 minute. The results are shown in Figure 2S and 3S

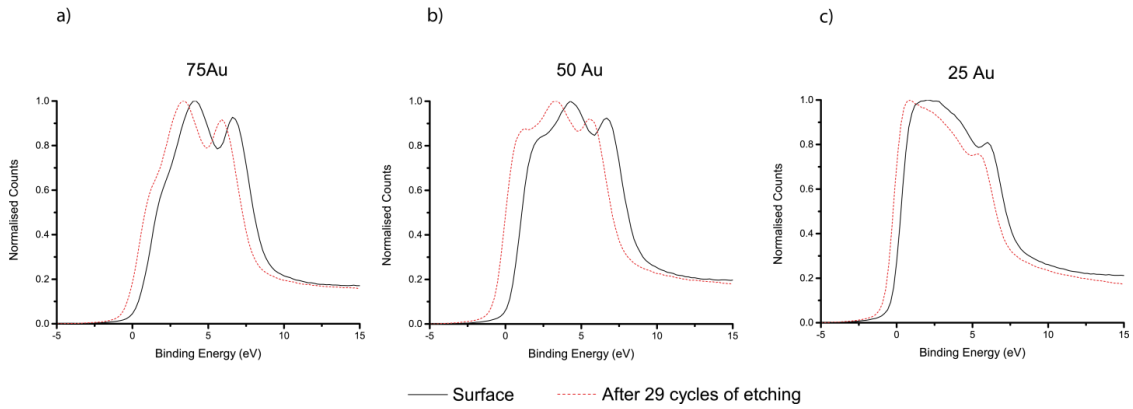

Figure 2S. XPS spectra of valence band of the sputtered surface (black solid) and the surface after 29 cycles of ion beam etching (red dotted) for Au-Pd thin films alloys with composition (a) $Au_{75}Pd_{25}$ (b) $Au_{50}Pd_{50}$ (c) $Au_{25}Pd_{75}$ prior to CO reduction.

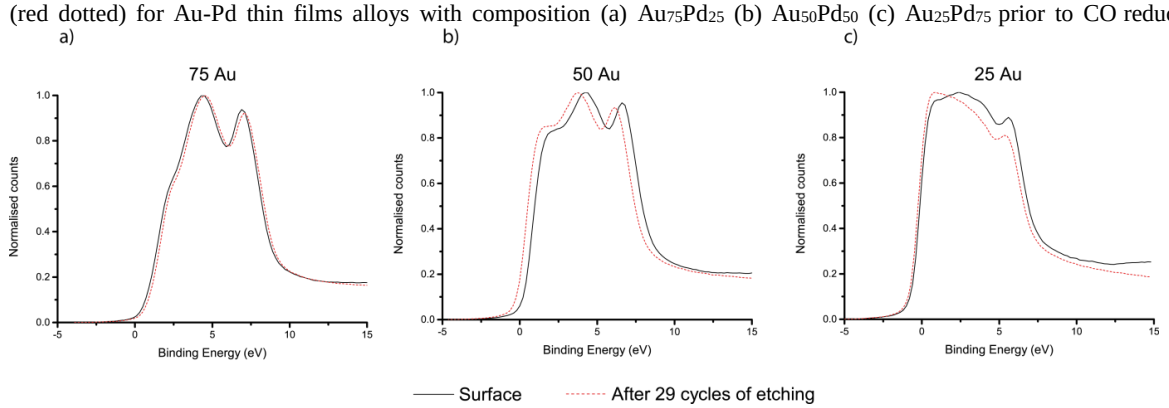

Figure 3S. XPS spectra of valence band of the sputtered surface (black solid) and the surface after 29 cycles of ion beam etching (red dotted) for Au-Pd thin films alloys with composition (a) $Au_{75}Pd_{25}$ (b) $Au_{50}Pd_{50}$ (c) $Au_{25}Pd_{75}$ after CO_2 reduction.

The surface after etching for 30 minutes can be considered as bulk from the fact that the carbon peak which was prominent before the start of the etching process almost disappeared after etching (Figure 4S). It must be also noted that the etching process does involving some mixing of components also.

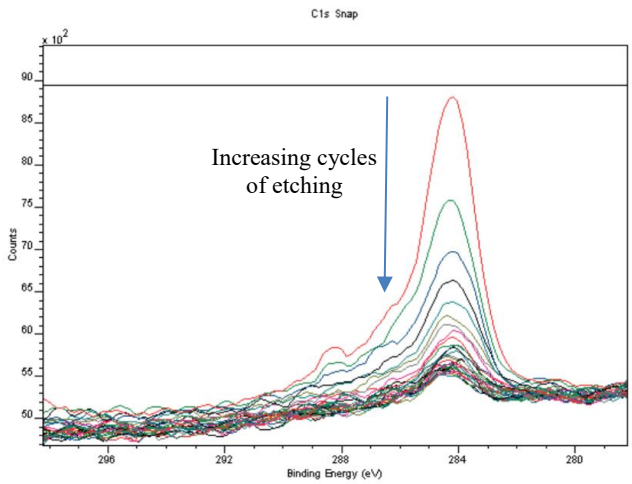

Figure 4S. XPS spectra of C species after each cycle of etching using ion beam for Au25Pd75. The carbon peak is found to reduce with etching confirming that the etching process takes places. The peak almost disappears by 29 cycles of etching.

SI-3. Surface composition using X-Ray Photoelectron spectroscopy (XPS)

The surface composition of the thin film alloys were calculated using both Au $4d_{3/2}$ – Pd $3d_{3/2}$ and Au $4p_{3/2}$ – Pd $3d_{3/2}$. The calculations were done for the electrodes before CO_2 reduction and after CO_2 reduction at -0.5 V. The results are shown in Table 2S and Table 3S.

Expected Composition	Using Au 4d 3/2 and Pd 3d 3/2	Using Au 4p 3/2 and Pd 3d 3/2
75%	77.66 %	75.57 %
50%	56.19 %	51.58 %
25%	19.14 %	16.37 %

Table 2S Composition of the Au-Pd thin film alloys before CO_2 reduction as calculated from XPS survey spectra. All values show % of Au content.

Expected Composition	Using Au 4d 3/2 and Pd 3d 3/2	Using Au 4p 3/2 and Pd 3d 3/2
75%	78.90 %	75.01 %
50%	56.15 %	47.59 %
25%	21.01 %	16.85 %

Table 3S Composition of the Au-Pd thin film alloys after CO_2 reduction at -0.5 V as calculated from XPS survey spectra. All values show % of Au content.

SI-4. Electrochemical Reduction of CO_2

All electrochemical experiments were carried out in a custom-made electrochemical cell with two compartments – working electrode compartment and the counter electrode compartment. The two compartments were separated by a Nafion 115 proton exchange membrane. Pt plate was used as the counter electrode and saturated Ag/AgCl was used as reference electrode. 0.1 M $KHCO_3$ (99.95%, Sigma Aldrich) solution was filled as electrolyte in both compartments. Prior to electrolysis, CO_2 was bubbled through the electrolyte in both compartments for 20 minutes at a flow rate of 15 ml min^{-1}. All electrolysis experiments were conducted at room temperature (25˚C) and 1 atm with pH of the electrolyte at 6.8. A potentiostat (Parstat 4000, Princeton Applied Research) was used to apply the potential versus the reference electrode which was later converted to RHE. The potentials applied were manually corrected for the ohmic drop. CO_2 was continuously purged throughout the experiment in both the electrolyte compartments. A magnetic stirrer rotating at 960 rpm was used in the working electrode compartment in order to effectively remove the gaseous products from the liquid phase. The gases from the cell were led into the sampling loop of a gas chromatograph (CompactGC 4.0, Global Analyser Solutions) with a run time of 3min 16s. Each electrolysis experiment was performed for 20 minutes and 5 GC injections were taken. The average of all 5 readings of the GC are used to calculate the FE which is reported. Due to similar roughness, the ECSA of the Pd electrode was used to calculate the current density of each of the electrodes (see supporting information SI-7)

Prior to performing CO_2 reduction experiments, chronopotentiometry was performed on Au in 0.1 M $KHCO_3$ without bubbling CO_2 . Since no CO_2 was bubbled through the electrolyte, only hydrogen is expected to be produced. The gases produced during electrolysis are periodically analyzed using gas chromatography (CompactGC 4.0, Global Analyser Solutions). The analysis confirms that only hydrogen is produced, and the faradaic efficiency calculations add up ~ 100% as shown in Figure 5S. The mean and standard deviation of the faradaic efficiencies are also estimated. The GC takes one reading for stable faradaic efficiency and concentration and hence atleast 3 readings are performed at each potential.

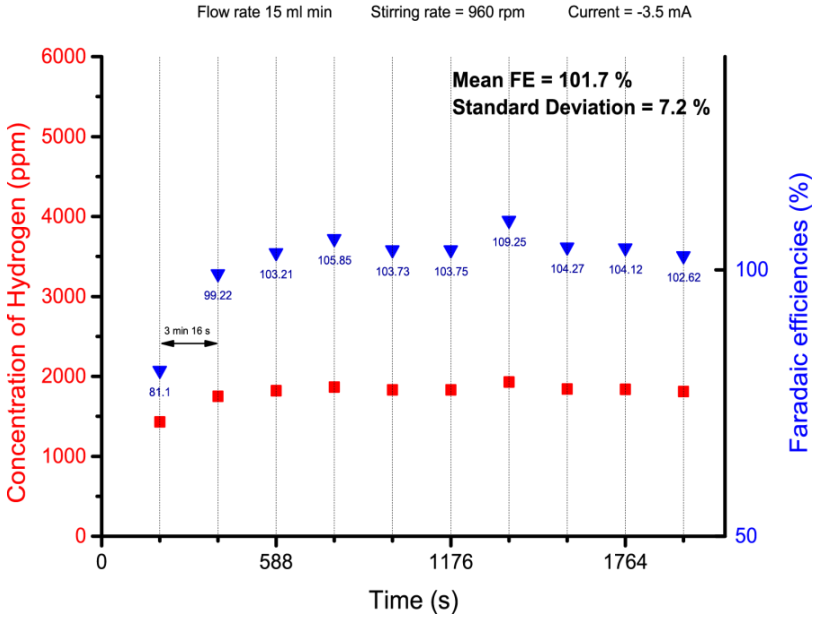

Figure 5S. Faradaic efficiencies and concentrations of hydrogen detected by the GC during the chronopotentiometry of pure Au thin film in 0.1 M $KHCO_3$ without bubbling CO_2 at -3.5 mA. The mean faradaic efficiency and its standard deviation are indicated in the figure. The flow rate of 15 ml min^{-1} and stirring rate of 960 rpm are used for all the CO_2 reduction experiments.

All electrochemical measurements were performed in a custom made electrochemical cell with two compartments (working and counter electrode compartments). The compartments were separated by a proton exchange membrane, Nafion 115. A three electrode configuration was used for all experiments with a Pt plate as counter electrode and saturated Ag/AgCl electrode as reference electrode. Both compartments were filled with 0.1 M $KHCO_3$ (99.95%, Sigma Aldrich). Prior to CO_2 reduction experiments, both compartments were purged with CO_2 at constant flow rate of 15 ml/min. The electrolyte was bubbled for 20 min to make it saturated with CO_2 (pH = 6.8). Chronoamperometry was started immediately after 20 min and the flow rate of CO_2 was kept constant throughout. Five GC injections were taken for each potential and the electrolysis was performed for ~20 minutes. The gaseous products were analysed using gas chromatography (CompactGC 4.0, Global Analyser Solutions). All mesurements were done at room temperature and atmospheric pressures. All potentials were applied versus saturated Ag/AgCl and converted to reversible hydrogen electrode (RHE) using the following equation.

$$E_{RHE} = E_{Ag/AgCl} + 0.197 + 0.0591 \times pH$$

SI-5. Hydrogen adsorption/absorption calculations

The charge per unit area required for the adsorption of a monolayer of hydrogen on Pd can be calculated using the amount of palladium per unit area. Each Pd atom is expected to bind to one H atom and the process involves a one electron (n).

Charge per unit area for H adsorption (Q) $= Nqn = 1.526 \times 10^{15} \times 1.602 \times 10^{-19} \times 1 = 244\ \mu C\ cm^{-2}$

Although the amount of charges calculated correspond to the adsorption of H on pure Pd, it might be different for alloys. However, it is reasonable to assume that charges of the same order of magnitude or lesser are indicative of adsorption while charges much greater than this is an indication of absorption. Since all the alloys were prepared by magnetron sputtering and the RMS roughness calculated from AFM show similar values, the area of all the electrodes is assumed to be the same.

Taking a suitable baseline, the area of the peaks corresponding to the hydrogen desorption are calculated from the respective voltammograms as shown in Figure 6S.

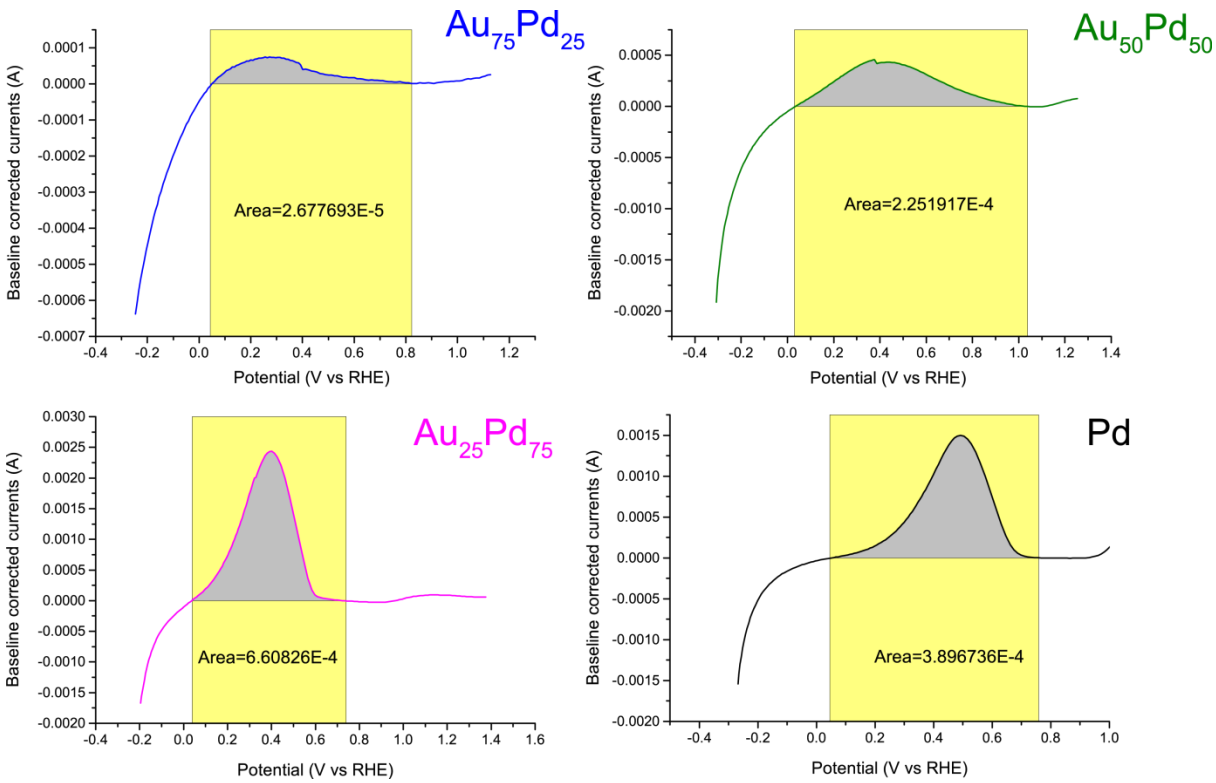

Figure 6S. Calculated areas for Au-Pd films in CO_2 saturated 0.1 M $KHCO_3$ corresponding to the hydrogen desorption peak in the cyclic voltammograms with cycling upto -0.4 V.

Using the calculated area and the scan rate, the total charges corresponding to the hydrogen desorption can be estimated. The total charges obtained for the different alloys and pure Pd are shown in

Table 4S.

Composition	Total charge (μC cm^{-2})
$Au_{75}Pd_{25}$	130
$Au_{50}Pd_{50}$	1091
$Au_{25}Pd_{75}$	3222
Pd	1885

Table 4S. Total charges corresponding to the hydrogen absorption/adsorption peak of Au-Pd alloys

The charges corresponding to the hydrogen desorption peak for Pd is larger than the value calculated for adsorption of hydrogen on Pd. The larger charges could be attributed to the absorption of hydrogen by Pd. It is known that Pd absorbs hydrogen which finds a direct application in diffusion membranes to purify H_2. The total charges for $Au_{50}Pd_{50}$ and $Au_{25}Pd_{75}$ are also larger than 244 μC cm^{-2} indicating that in these alloys also, hydrogen absorption occurs. The charge for hydrogen desorption in the $Au_{75}Pd_{25}$ alloy is much smaller than that calculated for hydrogen adsorption. This is a clear indication of the absence of hydrogen absorption.

SI-6. Cycling voltammetry of adsorbed intermediates

The relationship between the hydrogen absorption and the binding of CO2RR intermediates was studied using cyclic voltammetry of 25% Au electrode in CO_2 saturated 0.1 M $KHCO_3$. Initially, two scans were performed from 0.4 RHE to -0.9 RHE with the cathodic sweep first. The first scan showed a cathodic peak for the adsorbed intermediates as shown in Figure 7S.

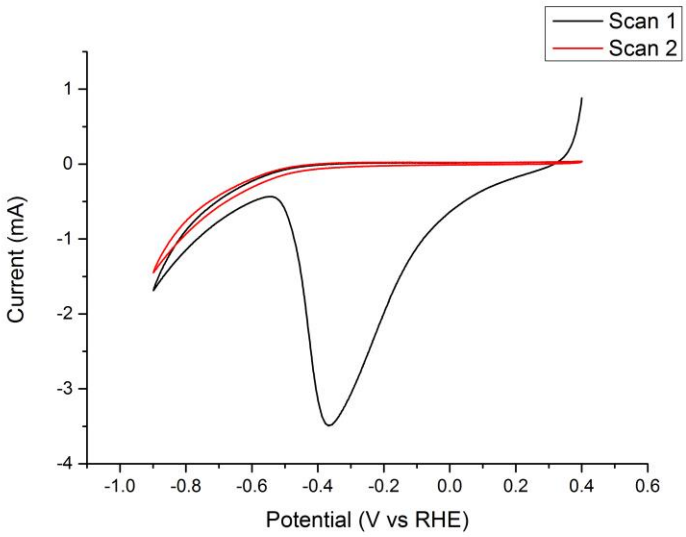

Figure 7S. Cyclic voltammetry of 25% Au electrode in 0.1 M $KHCO_3$ from 0.4 V to -0.9 V at scan rate of 0.05 V s^{-1}

The hydrogen absorption/adsorption region (0 to 0.4 V) was cycled to observe if hydrogen was adsorbed/absorbed or desorbed. The current in the nA range shown in Figure 8S confirm that no process takes place in this region.

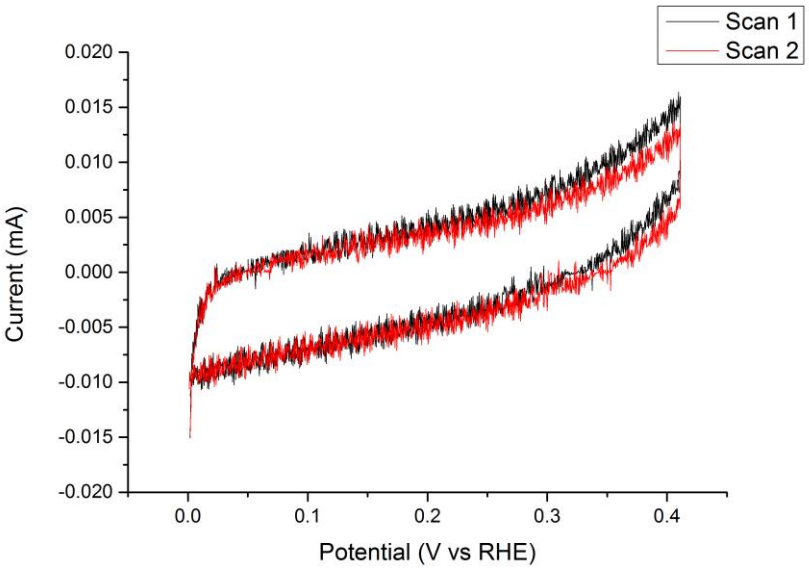

Figure 8S. Cyclic voltammetry of 25% Au electrode in 0.1 M $KHCO_3$ from 0 V to 0.4 V at scan rate of 0.05 V s^{-1}

On extending the potential range for the scan to 1.6 V, a sharp peak was observed ~1.2 V which corresponds to CO desorption. Another cycle in the same range leads to the appearance of a peak at 0.3 V as shown Figure 9S which corresponds to that of hydrogen desorption. This might lead to the conclusion that hydrogen desorption does not occur as the electrode surface is covered with CO_2. However, it must be noted that in Figure 9S, a broad peak at ~0.9 V overlaps with the sharp peak at ~1.2 V. The broad peak at 0.9 V in scan 1 probably corresponds to hydrogen desorption. The late appearance of this peak in this scan suggests that hydrogen desorption still occurs but is made more difficult by the adsorbed intermediates. Once these are removed, hydrogen desorption peak shifts back to its origin position. Thus it may be concluded that the hydrogen absorbed finds it difficult to escape out from the electrode when it is covered by the CO2RR intermediates.

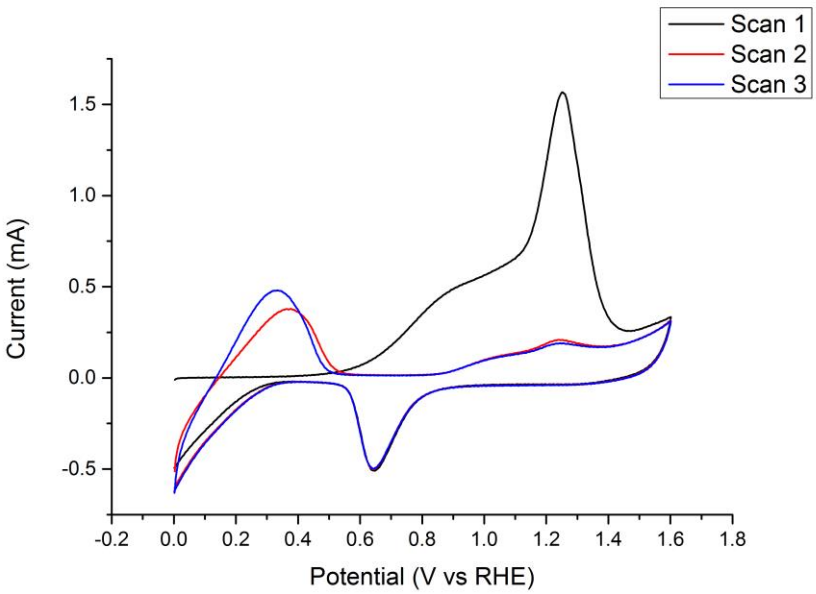

Figure 9S. Cyclic voltammetry of 25% Au electrode in 0.1 M $KHCO_3$ from 0 V to 1.6 V at scan rate of 0.05 V s^{-1}

SI-7. Electrochemical Surface Area (ECSA) calculations

The electrochemical surface area (ECSA) for the electrodes were calculated using the cyclic voltammogram of pure Pd. Pd forms a face centred cubic (FCC) crystal structure. The arrangement of atoms in a (111) crystal plane of a typical FCC crystal is shown in Figure 10S.

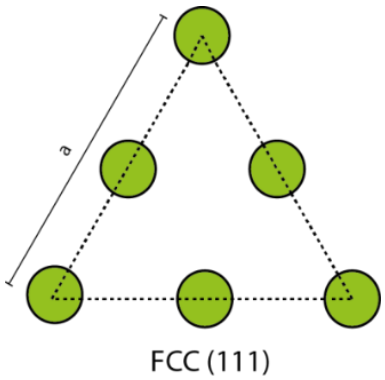

Figure 10S. Arrangement of atoms in a typical FCC crystal.

Number of atoms in the (111) plane $= \frac{1}{2} \times 3 + \frac{1}{6} \times 3 = 2$ atoms

Lattice parameter for Pd (a) = 389 pm = 3.89×10^{-8} cm

Number of atoms of Pd per unit area (N) $= \frac{2}{\frac{\sqrt{3}}{2}a^2} = \frac{2}{\frac{\sqrt{3}}{2}(3.89 \times 10^{-8})^2} = 1.526 \times 10^{15}$ atoms/cm^2.

Since the reduction peak corresponds to PdO is being reduced to Pd, two electrons (n=2) are involved in the process. The charge of one electron (q) is 1.602×10^{-19} C.

Total charges per unit area for reduction $= Nqn = 1.526 \times 10^{15} \times 1.602 \times 10^{-19} \times 2 = 488\ \mu C\ cm^{-2}$

The CV of pure Pd in the absence of CO_2 is taken to calculate the total charge corresponding to the reduction of PdO to Pd as shown in Figure 11S. A scan rate of 0.05 V s^{-1} was used for the cyclic voltammetry.

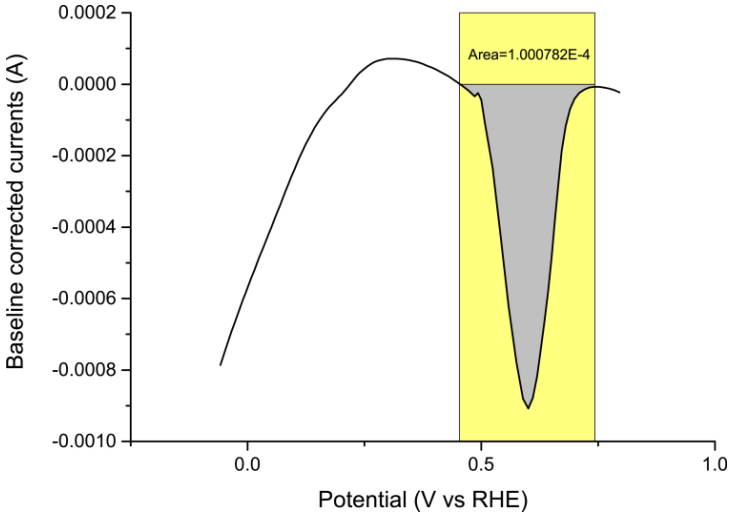

Figure 11S. Area of the reduction peak of Pd in 0.1 M $KHCO_3$ without CO_2 bubbling

Total charges from CV $= \frac{Area\ of\ the\ peak}{Scan\ rate} = \frac{0.000100782}{0.05} = 2015\ \mu C$

ECSA of the thin films $= \frac{Total\ charges\ from\ CV}{Total\ charges\ per\ unit\ area\ for\ reduction} = \frac{2015}{488} = 4.12\ cm^{-2}$

SI-8. X-Ray Diffraction (XRD)

X-ray diffraction was used for the characterization of all the Au-Pd alloys. The lattice parameter for all the compositions were calculated using the following equation.

$$a = \frac{\sqrt{3}\,\lambda_{cobalt}}{2\sin\theta}$$

where θ is the angle between the incident X-ray and the scattering planes and λ_{cobalt} is 0.178897 nm.

XRD patterns of all the alloys are shown in Figure 12S and the lattice parameters are tabulated in Table 5S. The lattice parameters of Au and Pd closely match with the reported values.

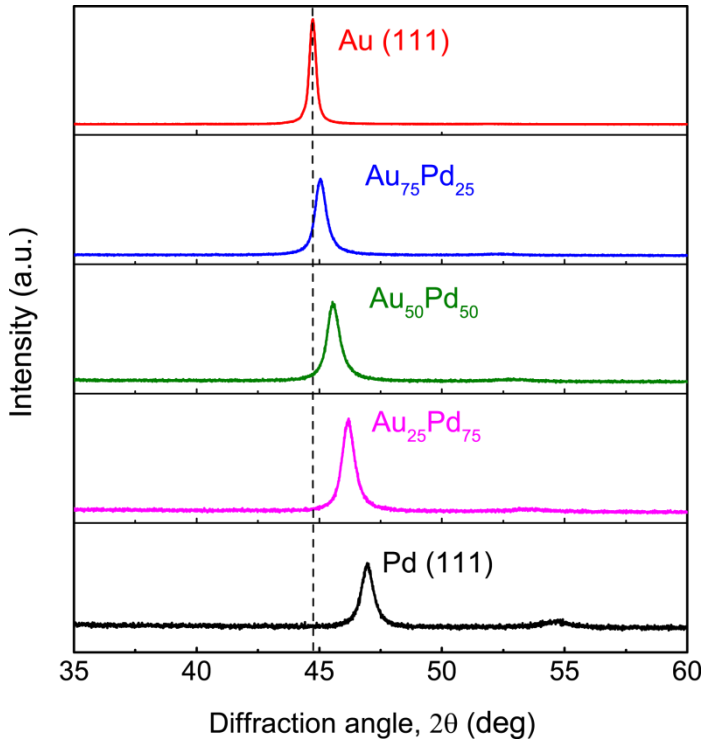

Figure 12S. X-ray diffraction (XRD) patterns of pure Au, pure Pd and Au-Pd thin film alloys (FCC, 50 nm thickness) of different compositions using Co-Kα (λ=0.178897 nm). The peak is found to shift gradually on increasingly adding Pd to Au.

Composition	Lattice parameter (A^0)
Au	4.071464
$Au_{75}Pd_{25}$	4.043865
$Au_{50}Pd_{50}$	4.002828
$Au_{25}Pd_{75}$	3.948924
Pd	3.884979

Table 5S. Lattice parameter as calculated using XRD for all compositions of Au-Pd alloys

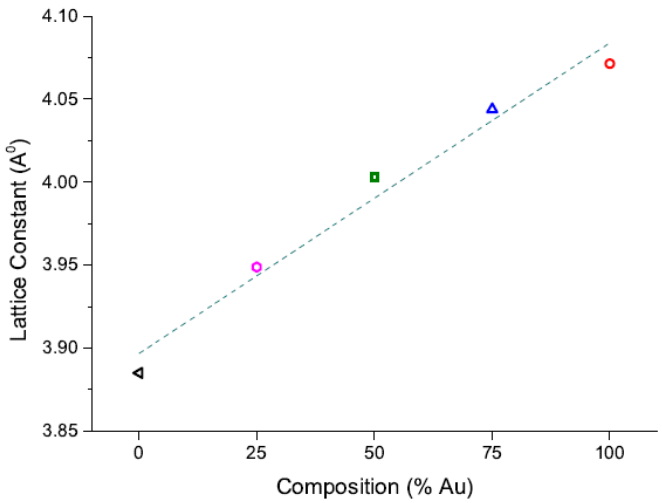

Figure 13S Lattice parameter as a function of the composition. The lattice expands almost linearly with composition thus verifying Vegard's law.

SI-9. in-situ surface enhanced infrared absorption spectroscopy (SEIRAS)

We studied the electrochemical reduction of CO2 on sputtered palladium thin films, using in-situ surface enhanced infrared absorption spectroscopy (SEIRAS) to better understand the interaction of Pd with CO_2 reaction intermediates. Cyclic voltammetry measurements were performed between -0.8 V and 1.2 V vs RHE with a scan rate of 10 mV/s while simultaneously measuring with in-situ SEIRA measurements (Figure 7a and 7b). Notably, sweeping in cathodic direction gave rise to a reduction peak centered around -0.2 V vs. RHE which coincides very well the initiation of bridge bonded CO formation on Pd surface inferred from SEIRA spectra. On the contrary of expected vibrational Stark effect, sweeping to more negative potentials exhibited a shift to higher wavenumbers in CO band untill -0.5 V vs. RHE. CO interacts with metal bands dominantly via anti-bonding 2π* and bonding 5σ orbitals. Since 5σ orbitals are spatially localized at the carbon end of the molecules, the effect of metal and 5σ orbital interaction on the CO bond strength is small. Therefore, CO bond strength and correspondingly stretching frequency is dominated by the interaction of metal bands with 2π* orbitals.[1] Sweeping potentials in the negative direction usually leads to a decrease in the stretching frequency as a result of back-donation of electrons from metal to 2π* orbitals. The increase in the stretching frequency of CO bond in this case, therefore, is considered to be a result of the dipole-dipole coupling between CO molecules at neighboring sites. This is very well supported by applying a constant potential onto Pd electrode to exclude any effect of potential modulation while monitoring the frequency of the CO band (Figure 7c). The increase in the frequency of CO bond clearly comply with the decrease in the current transient at -0.3 V vs. RHE. This highly suggests that the dense patches of interacting CO molecules are formed on Pd surface under cathodic conditions (>-0.6 V vs. RHE) in a short amount of time. A noticeable decrease in the frequency of CO bond below -0.5 V vs RHE is in very well agreement with the detection of appreciable amount of CO on the headspace at these potentials in this study and literature suggesting the release of CO molecules and a corresponding decrease on the coverage.[2]

CO band frequency exhibited a clear and steady increase while sweeping back from -0.8 V vs RHE to less negative potentials as the vibrational stark effect and dipole-dipole coupling corroborate each other. The large hysteresis in the cathodic part of voltammetry curve was a result of dramatic decrease in HER on CO covered surface. The stark tuning slopes in this potential range most likely influenced by changes in CO coverage so it is not possible to get a reliable number. Considering the formation of CO is minimal at anodic potentials, stark tuning slopes can be extracted for a specific coverage from change in the frequency of CO band between 0V and +0.6 V vs RHE. However, this most likely will be highly dependent on how potential is modulated cathodically. Higher anodic potentials above 0.6 V vs. RHE resulted in the anodic stripping of CO evident from decrease and following disappearance of CO band. The adlayer structure of CO on Pd is considerably complex and highly depends on the coverage. In-situ electrochemical STM and/or systematic SEIRAS studies with mixtures of $^{12}CO_2/^{13}CO_2$ are necessary to understand the adlayer structure of Pd and its alloys which requires an extensive independent study.[3]

SI-10. Kinetic Model

$$H_2O + e^- + * \overset{K_{vol}}{\longleftrightarrow} {}^*H + OH^-$$

$${}^*H + H_2O + e^- \xrightarrow{k_{hey}} H_{2\,(g)} + OH^- + *$$

$${}^*CO_2 + H_2O + e^- + * \overset{K_{CO2RR_1}}{\longleftrightarrow} {}^*COOH + OH^-$$

$${}^*COOH + H_2O + e^- \overset{K_{CO2RR_2}}{\longleftrightarrow} {}^*CO + OH^- + H_2O$$

$${}^*CO \xrightarrow{k_{CO2RR_3}} CO_{(g)} + *$$

The model is based on the pseudo-steady state approximation (PSSA), which assumes that under steady state conditions the coverages of vacant sites (θ_*), COOH (θ_{*COOH}), CO (θ_{*CO}), and H (θ_{*H}), do not change with time. This way the following equations can be derived by applying the PSSA to each adsorbed species in the above set of reactions.

$$\frac{d\theta_{*H}}{dt} = 0 = r_{vol} - r_{-vol} - r_{hey}$$

$$\frac{d\theta_{*COOH}}{dt} = 0 = r_{CO2RR_1} - r_{-CO2RR_1} - r_{CO2RR_2} + r_{-CO2RR_2}$$

$$\frac{d\theta_{*CO}}{dt} = 0 = r_{CO2RR_2} - r_{-CO2RR_2} - r_{CO2RR_3}$$

where $r_{vol}, r_{Hey}, r_{CO2RR_1}, r_{CO2RR_2}$ and r_{CO2RR_3}, are the forward reaction rates of the reactions shown above, r_{-CO2RR_1} and r_{-CO2RR_2} are the corresponding backward reactions and θ is the coverage of each species.

From these equations and knowing that $\theta_{*CO} + \theta_{*COOH} + \theta_{*H} + \theta_{*} = 1$, the following expressions for the coverages can be obtained:

$$\theta_{*CO} = \frac{1}{1 + \left[\frac{1}{\gamma_{COOH} \cdot \gamma_{CO}}\right] + \left[\frac{1}{\gamma_{CO}}\right] + \left[\frac{\gamma_H}{\gamma_{COOH} \cdot \gamma_{CO}}\right]}$$

$$\theta_{*} = \frac{\theta_{*CO}}{\gamma_{COOH} \cdot \gamma_{CO}}$$

$$\theta_{COOH} = \frac{\theta_{*CO}}{\gamma_{CO}}$$

where,

$$\gamma_{COOH} = \frac{k_1 \cdot x_{CO_2}}{k_{-1} \cdot x_{OH} + k_2 - k_{-2} \cdot \gamma_{CO} \cdot x_{OH}}$$

$$\gamma_{CO} = \frac{k_2}{k_{-2} \cdot x_{OH} + k_3}$$

$$\gamma_H = \frac{k_{vol}}{k_{-vol} \cdot x_{OH} + k_3}$$

where x_{OH} and x_{CO_2} are the concentrations of OH^- and dissolved CO_2, which were assumed to be bulk concentrations at the experimental conditions (0.1 M KHCO3 at pH = 6.85). And the rate constants are represented by the symbol k, which is a function of the activation energies:

$$k = c^{sites}\left(\frac{k_B T}{h}\right) exp\left[-\frac{\Delta G^{act,0}}{k_B T}\right]$$

where c^{sites} is the concentration of active sites, k_B is the Boltzmann constant, T is the temperature, h is the Planck constant, and $\Delta G^{act,0}$ is the activation energy. The activation energy used in this equation significantly differs from the real activation energy since this equation assumes a transmission coefficient equal to one and the concentration of sites is assumed to be that of a monocrystalline gold. Therefore, this activation energy is an apparent activation energy, whose applied potential dependence can be used in the above model to simulate the potential and material dependency of the coverages and partial currents. The potential dependency in this model is assumed to be linear:

$$\Delta G^{act,0} = a + b(E - E_{onset})$$

where, E is the applied potential and E_{onset} is the onset potential for each elementary reaction. By setting the parameters a and b for each elementary reaction one can solve for the potential dependent coverages and partial currents.

The parameters used in the model to obtain Figure 8 and 9 in the main manuscript are the following:

	Au	AuPd (low Pd content)	AuPd	AuPd (high Pd content)
a vol	0.78	0	0	0
a hey	0.05	0.78	0.8	0.81
b vol	0.2	0.2	0.2	0.2
b hey	0.2	0.2	0.2	0.2
a CO2RR1	**0.28 (RDS)**	**0**	**0**	**0**
a CO2RR2	**0.05**	**0.3**	**0.3**	**0.3**
a CO2RR3	**0.05**	**0.69 (RDS)**	**0.71 (RDS)**	**0.73 (RDS)**
b CO2RR1	0.2	0.2	0.2	0.2
b CO2RR2	0.2	0.2	0.2	0.2
$Eonset$ vol	-0.3 V vs. RHE	0	0	0
$Eonset$ hey	-0.3 V vs. RHE	0	0	0
$Eonset$ CO2RR1	-0.3 V vs. RHE	-0.3 V vs. RHE	-0.3 V vs. RHE	-0.3 V vs. RHE
$Eonset$ CO2RR2	-0.3 V vs. RHE	-0.3 V vs. RHE	-0.3 V vs. RHE	-0.3 V vs. RHE

$Eonset$ **CO2RR3**	-0.3 V vs. RHE	-0.3 V vs. RHE	-0.3 V vs. RHE	-0.3 V vs. RHE

The above arbitrary parameters were set with the purpose to understand the HER suppression effect seen experimentally. The model assumes that the rate determining step (RDS) for Au is the CO_2 adsorption step, while for the alloys is the desorption step. Therefore, the largest parameter a for each composition corresponds to the parameter of the RDS reaction, which corresponds to the largest activation energy in the energy landscape of the reaction. The only parameter changed while modeling different alloys was the a parameter of the CO release step (RDS). The analysis given in the main manuscript shows that just by changing this parameter the site competition effect in the HER suppression can be identified and analyzed. The phenomenological onset potential (Eonset) for CO2RR were all set to the same reference value (-0.3 V vs. RHE). Any other value could be used as potential reference (Eonset) and the only effect would be to shift the apparent activation energy by $b(E - E_{onset})$. The Eonset for the HERs for the alloys are purposely set to zero to explicitly account for the drastic proton adsorption onset potential difference between Au and the alloys.

All the a_{CO2RR2} and b values shown in the table were set to match the order of magnitude of the currents that were obtained experimentally. For example, the values for a_{CO2RR2} were initially set to 0.2 for all the alloys and Au, making sure that these values do not exceed the a parameters of the corresponding RDS reactions. However, as it can be seen in Figure 14S, the a_{CO2RR2} =0.2 for Au results in an extremely high CO partial current at lower potentials that is not seen experimentally (Figure 5b). This relatively high a_{CO2RR2} value stabilizes the COOH intermediate and results in an increase of the intermediate coverage, which in turn results in a higher CO current. In order to obtained CO currents of the same order of magnitude as those measured (Figure 5b), the a_{CO2RR2} for Au is decreased to 0.05 (Figure 14S), which results in (i) negligible COOH coverages and (ii) CO partial currents of the same order of magnitude as those found experimentally. The alloys do not change significantly the coverages and partial currents by changing the a_{CO2RR2} from 0.2 (Figure 14S) to 0.3 (Figure 9b in the main manuscript).

Finally, all the a and b parameters for the equilibrium constants (K) were set to 0.5. The equilibrium constants (K) were used to calculate the backward reaction constants (k_{back}) of the Volmer reaction, CO2RR1 and CO2RR2 as follows:

$$k_{back} = \frac{k_{for}}{K},$$

where,

$$K = exp\left[-\frac{\Delta G^0}{k_B T}\right]$$

where,

$$\Delta G^0 = a + b(E - E_{onset})$$

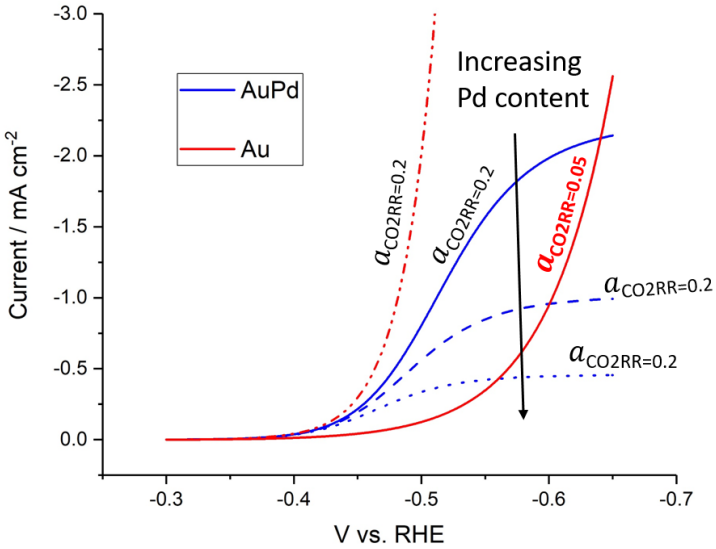

Figure 14S. Comparison between CO partial currents for Au modeled with α_{CO2RR2}=0.2 and α_{CO2RR2}=0.05. The α_{CO2RR2} = 0.05 yields currents of the same order of magnitude than those measured experimentally.

SI-11. Sputtering of thin films

Magnetron co-sputtering technique was used to synthesize all thin film electrodes. Two targets, Au and Pd of high purity were used whose sputter rates were calculated prior to synthesizing the alloys. DC power supply was connected to two sputter guns. A pressure of 3 µbar was applied along with an Ar flow of 20 sccm. Prior to sputtering, a 2 min cleaning step was performed by providing a bias to the substrate. Depending upon the composition of the alloy, the power supplied to the sputter guns were controlled and the time required for co-sputtering was calculated. The substrate was rotated to ensure a uniform film thickness. The sputtering was performed at room temperature. The shutters of the sputter guns were closed in the order Pd followed by Au.

References

1. Kolasinski, K. W. *Surface Science: Foundations of Catalysis and Nanoscience*. (Wiley, 2012).

2. Gao, D. *et al.* Pd-Containing Nanostructures for Electrochemical CO2 Reduction Reaction. *ACS Catal.* **8,** 1510–1519 (2018).

3. Wieckowski, A. *Interfacial Electrochemistry: Theory: Experiment, and Applications*. (Routledge, 2017).